Journal of Molecular Catalysis A: Chemical 311 (2009) 7–16

Contents lists available at ScienceDirect

Journal of Molecular Catalysis A: Chemical

journal homepage: www.elsevier.com/locate/molcata

Editor's choice paper

Effect of support and cobalt precursors on the activity of $Co/AlPO_4$ catalysts in Fischer–Tropsch synthesis

Jong Wook Bae, Seung-Moon Kim, Suk-Hwan Kang, Komandur V.R. Chary, Yun-Jo Lee, Hyo-Jin Kim, Ki-Won Jun*

Petroleum Displacement Technology Research Center, Korea Research Institute of Chemical Technology (KRICT), P.O. Box 107, Yuseong, Daejeon 305-600, Republic of Korea

ARTICLE INFO

Article history:
Received 2 April 2009
Received in revised form 19 June 2009
Accepted 9 July 2009
Available online 18 July 2009

Keywords:
Fischer–Tropsch synthesis
Aluminum phosphate ($AlPO_4$)
Cobalt precursor
Filamentous carbon
Deactivation

ABSTRACT

Cobalt supported on amorphous aluminum phosphate ($Co/AlPO_4$) catalysts were prepared by the impregnation method using three different cobalt precursors such as cobalt nitrate, acetate and chloride to elucidate the activity of Fischer–Tropsch synthesis. The use of $AlPO_4$ as a support for cobalt-based catalysts exhibits better catalytic performance during FTS reaction than the corresponding Co/Al_2O_3 catalyst. TPR results also suggest that the reducibility of the catalysts varies with the nature of cobalt precursors employed during the impregnation on $AlPO_4$ support. The $Co/AlPO_4$ catalyst prepared from cobalt nitrate shows higher CO conversion and C_8+ selectivity than the others due to the facile formation of homogeneous cobalt particles with proper electronic characters and high reducibility. Interestingly, all $Co/AlPO_4$ showed a growth of filamentous carbon initiated from the large mobile cobalt particles during the reaction. The differences in catalytic properties of $Co/AlPO_4$ are mainly attributed to the cobalt particle size, reducibility with different electronic states of metallic cobalt, pore diameter of $AlPO_4$ and formation of filamentous carbon.

1. Introduction

Fischer–Tropsch synthesis (FTS) is one of the potential chemical routes to convert coal or natural gas to environmentally benign fuels with low emission of SOx and NOx and particulates and useful chemicals as well [1–7]. This process is becoming more and more attractive in recent years due to the depletion of oil resources in near future. Cobalt dispersed on metal oxide supports such as alumina or silica and promoted with noble metals is considered to be the most promising catalysts for the FTS reaction. Supported cobalt catalysts show high activity and selectivity to linear paraffins, possess high resistance towards deactivation, and also exhibit low activity for the water-gas shift reaction. The support plays an important role in dispersing the active cobalt metal and in changing the reducibility of cobalt species. The design of highly dispersed cobalt-based catalysts for FTS reaction on porous supports such as Al_2O_3 [7–11], TiO_2 [11], SiO_2 [12–16] has been numerously investigated. The reactivity of cobalt-based catalysts during FTS depends mainly on the cobalt particle size, dispersion of cobalt species, their reducibility and the nature of the support. Promoters like Ru, Re and Pt in combination with cobalt have shown a remarkable enhancement of the catalyst performance [17,18]. Moderating the interaction of cobalt with the support is also a favorable property in achieving high activity and selectivity during FTS reaction due to the ease of reduction of cobalt oxides. Metal–support interaction may leave a fraction of cobalt chemically inactive after reduction treatment. Saib et al. [19] have shown the higher reducibility of cobalt oxides in wide pore silica supported catalysts than with cobalt deposited in narrow pore structured supports. Khodakov et al. [20–22] have also shown that the ease of reduction decreases from large pores to smaller pores on silica supported cobalt catalysts. In recent years aluminum phosphate is receiving considerable attention as a support for a variety of catalytic reactions [23–30]. For examples, $AlPO_4$ is used as a support for nickel catalyst used in hydrogenation reactions [23]. For oxidation reactions, it is also used to support vanadium–phosphorus oxide catalysts [24]. $AlPO_4$, in combination with alumina, is also used as a support for nickel catalysts for partial oxidation and carbon dioxide reforming of methane [25] and dehydration of methanol to dimethyl ether [26,27]. High surface area and the large average pore size are the main reasons for using amorphous $AlPO_4$ as support. Amorphous aluminum phosphate is built of tetrahedral units of AlO_4 and PO_4 and is structurally similar to silica. The specific interaction with the supported species and $AlPO_4$ can be achieved by using proper synthesis procedures [28–30], and their catalytic properties may be improved. In addition, the phosphorous modification of hydrotreating catalysts is widely investigated by many researchers and their positive effects are related to the stabilization of active species by forming M-P oxo-

* Corresponding author. Tel.: +82 42 860 7671; fax: +82 42 860 7388.
E-mail address: kwjun@krict.re.kr (K.-W. Jun).

1381-1169/$ – see front matter © 2009 Elsevier B.V. All rights reserved.
doi:10.1016/j.molcata.2009.07.011

species (M = Co, Mo, Ni), by generating active sites with structural modification of catalyst, and by suppressing the metal–support interaction due to the strong affinity between Al and P resulted in enhancing the reducibility of active metal species [31]. It has been widely investigated that the structural and surface reduction properties of Co/SiO_2 are influenced by the nature of the cobalt precursor thus changing the adsorption properties during impregnation, by altering the exothermicity of precursor decomposition and eventually resulting in the variation of metal–support interaction [2,14,15,17]. The formation of Co_3O_4 on SiO_2 is more favorable on nitrate-derived cobalt and it is difficult to reduce when the catalyst is prepared using acetate precursor. Although cobalt chloride is easy to be reduced at low temperature like cobalt nitrate, its reoxidation to Co^{2+} is more facile during the FT reaction resulting in reduction of the activity and being easily poisoned by the residual chloride ions [7,14,15].

In the present investigation, we report the use of an amorphous $AlPO_4$ as a new supporting material for the cobalt-based catalysts in FTS reaction due to their characteristics of large pore diameter and low interaction with active metal species. Furthermore, the structure and catalytic properties of cobalt supported on $AlPO_4$ with different cobalt precursors have been investigated and characterized by the measurement of surface area and pore size distribution, X-ray diffraction (XRD), transmission electron microscopy (TEM), temperature programmed reduction (TPR), Fourier-transformed infrared (FT-IR) spectroscopy, H_2 chemisorption and X-ray photoelectron spectroscopy (XPS). The aim of this investigation is to find out the effect of the novel support $AlPO_4$ and the nature of cobalt precursors on the catalytic functionalities of cobalt supported on amorphous $AlPO_4$ during the FTS reaction such as CO conversion, selectivity to hydrocarbons and filamentous carbon formation.

2. Catalyst preparation and characterization

2.1. Catalyst preparation and activity test

Amorphous aluminum phosphate with a P/Al ratio of 0.9 was prepared from $Al(NO)_3{\cdot}6H_2O$ and $(NH_4)_2HPO_4$ by the following reported procedures. The starting materials were dissolved in deionized water (400 ml of 0.5 M of Al nitrate solution and 350 ml of 0.5 M of $(NH_4)_2HPO_4$ solution) and acidified with nitric acid. A hydrogel was then formed by adding 700 ml of 10% solution of ammonia to the acidified solutions of Al and P precursors until a pH of 8.0 was achieved. After 1 h, the contents were filtered and the hydrogel was washed with twice its volume of distilled water. The hydrogel was dried at 110 °C for 16 h and calcined at 500 °C in air for 0.5 h. The resulting aluminum phosphate support had a BET surface area of 173 m^2/g. The 20 wt.%$Co/AlPO_4$ catalysts were prepared by the conventional impregnation method with an aqueous solution containing three different cobalt precursors such as cobalt (II) nitrate, cobalt (II) acetate or cobalt (II) chloride. The notation of $Co/AlPO_4$ catalysts represents the kind of cobalt precursor employed during the preparation, e.g. catalysts prepared from cobalt nitrate, acetate and chloride are denoted as CoN, CoA and CoCl, respectively. For comparison, CoN–Al catalyst was made by using the Al_2O_3 support (Catapal B with a surface area of 200 m^2/g supplied by Sasol) from cobalt nitrate precursor. The supported cobalt catalysts were subsequently dried at 110 °C for 16 h and calcined at 500 °C for 5 h in air at a heating rate of 10 °C/min.

Prior to activity tests, the catalysts were activated at 400 °C in a fixed-bed reactor (I.D. = 12.7 mm) for 12 h with 5%H_2/He gas mixture. The activity test was carried out at differential conditions to minimize a hot-spot formation during the reaction such as catalyst loading of around 0.3 g with a particle size of 80–120 μm and its bed-height of around 5 mm. The activity test was conducted for more than 80 h under the following reaction conditions; Reaction T = 220–240 °C; P = 2.0 MPa; SV (1/kg_{cat}/h) = 2000; feed composition of $H_2/CO/CO_2/Ar$ (mol%) = 57.3/28.4/9.3/5.0 (selected as a model gas composition without CO_2 separation after steam carbon dioxide reforming with methane reaction of natural gas). The effluent gas from the reactor was analyzed by an online gas chromatograph (YoungLin Acme 6000 GC) employing GS-GASPRO capillary column connected with flame ionization detector (FID) for the analysis of the hydrocarbons and Porapak Q/molecular sieve (5A) packed column connected with thermal conductive detector (TCD) for the analysis of carbon oxides and hydrogen with an internal standard gas of Ar. The CO conversion from TCD analysis and product distribution from FID analysis are calculated based on the carbon balance by the following equations

$$\text{CO conversion (C-mol\%)} = \left[\frac{\text{moles of inlet CO} - \text{moles of outlet CO}}{\text{moles of inlet CO}}\right] \times 100$$

$$\text{Hydrocarbon } (Cx;\ x = 1,\ 2\text{–}4,\ 5\text{–}7 \text{ and } 8+) \text{ selectivity (C-mol\%)} = \left[\frac{\text{moles of Cx produced}}{\text{moles of inlet CO} - \text{moles of outlet CO}}\right] \times 100$$

2.2. Catalyst characterization

The BET surface area, pore volume and pore size distribution were estimated from nitrogen desorption isotherm obtained at −196 °C using a constant-volume adsorption apparatus (Micromeritics, ASAP-2400). The pore volume was determined at a relative pressure (P/P_0) of 0.99. The calcined samples were degassed at 300 °C in a He flow for 4 h before the measurements. The pore size distribution of the samples was calculated using the BJH (Barett–Joyner–Halenda) model from the data of desorption branch of the nitrogen isotherms.

The powder XRD patterns of samples were obtained on a Rigaku diffractometer using Cu K_α radiation operating at 40 kV and 40 mA with a scanning rate of 5°/min from 5° to 80° to identify the crystalline phases of $Co/AlPO_4$ catalysts. The calcined samples as well as those reduced at 400 °C for 12 h with 5 vol.% H_2/N_2 flow, followed by passivation with 0.1%O_2/He for 0.5 h at room temperature (RT), were characterized separately to identify the crystalline phases of Co_3O_4, CoO and Co metal. The identification of crystalline phases of cobalt species was made with the help of Joint Committee on Powder Diffraction Standards files (JCPDS) for Co_3O_4 with JCPDS card number of 78-1969 and Co with that of 89-4308. The surface morphology and compositions of $Co/AlPO_4$ were measured by using the scanning electron microscope (SEM; JEOL (JSM6700F)) and energy dispersive spectroscopy (EDS). Furthermore, the used $Co/AlPO_4$ catalysts were also characterized by using TEM (TECNAI G2 instrument) analysis operating at 200 kV.

The TPR experiment was performed to determine the reducibility of the surface Co_3O_4 species. Prior to the TPR experiments, the sample was pretreated in a He flow up to 350 °C and kept for 2 h to remove the adsorbed water and other contaminants followed by cooling to 50 °C. The reducing gas of 5 vol.% H_2/He was passed over the samples at a flow rate of 30 ml/min with a heating rate of 10 °C/min up to the 750 °C and kept at that temperature for 0.5 h. The effluent gas was passed over a molecular sieve trap to remove the generated water and analyzed by GC equipped with TCD.

The FT-IR spectra of calcined samples were recorded on a Nicolet Protege 460 FT-IR spectrometer equipped with a MCT detector which was cooled with liquid nitrogen and at a spectral resolution of 2 cm^{-1}. The collected spectra of calcined samples were obtained

by subtraction of blank spectra from the calcined $Co/AlPO_4$ samples. The diffuse reflectance infrared Fourier transform (DRIFT) of adsorbed CO molecule on reduced catalysts was also conducted on the same instrument. All catalysts were previously reduced in situ at 400 °C for 12 h under 5 vol.% H_2/He flow. The reduced catalyst was kept at that temperature for 1 h and cooled to 50 °C under He flow to remove H_2 on the cobalt surface. And then, CO was introduced at 50 °C for 0.5 h with a flow rate of 30 cm^3/min and the CO gas was switched with He again to remove the gaseous CO molecules. The FT-IR spectra of adsorbed CO molecules were obtained by subtracting that of reduced catalyst. FT-Raman spectra were recorded under ambient conditions using a Bruker FRA106/S with the excitation laser of Nd:YAG (wavelength of 1064 nm) and optical power of 300 mW at the sample position.

The dispersion of cobalt and cobalt metal surface area was measured by H_2 chemisorption at 100 °C under static conditions using micrometrics ASAP 2000 instrument equipped with a high vacuum pump system providing 10^{-6} Torr. Prior to adsorption measurements, the sample (0.5 g) was reduced in situ at 400 °C for 12 h under 5 vol.% H_2/N_2 flow. H_2 chemisorption uptakes were determined as the difference of two successive isotherms measured. In each case, the difference of the two isotherms extrapolated to zero pressure was considered as the amount of chemisorbed hydrogen molecules. The metal dispersion and cobalt metal surface area were calculated with the assumption of H/Co metal's stoichiometry of 1.0. The reduction degree of samples was determined by O_2 titration method and then the particle size of cobalt metal was corrected by considering the reduction degree. The reduction degree was determined by the following equation; [the amount of O_2 consumption (mmol O_2; $3Co + 2O_2 \rightarrow Co_3O_4$)]/[the theoretical amount of H_2 consumption with the assumption of fully reduced cobalt oxides (mmol H_2; $Co_3O_4 + 4H_2 \rightarrow 3Co + 4H_2O$)] × 100).

The surface cobalt species after calcination were characterized by using the XPS (ESCALAB MK-II). During the experiments, the Al K_α monochromatized line (1486.6 eV) was adopted and the vacuum level was around 10^{-7} Pa. The calcined powder sample was previously pressed to thin pellet and the binding energy (BE) was corrected with the reference BE of C 1s (284.4 eV).

3. Results and discussion

3.1. Textual properties of $Co/AlPO_4$ catalysts

The textural properties of $AlPO_4$ and $Co/AlPO_4$ Fischer–Tropsch catalysts are given in Table 1 and Fig. 1. The laboratory-made $AlPO_4$ shows a surface area of 173 m^2/g and average pore diameter of around 19.4 nm. Its surface area decreases considerably after impregnation of cobalt on $AlPO_4$. The CoN catalyst has shown higher surface area than CoA and CoCl catalysts. For comparison, the CoN–Al catalyst shows a surface area of 139 m^2/g and smaller average pore diameter of around 6.7 nm. The decrease in surface area after cobalt addition is probably due to its deposition in inner pores of $AlPO_4$ or blockage of small pore by the formation of cobalt oxide particles. The decrease in surface area is much severe in CoA catalyst. The dilution effect caused by very low surface area of cobalt oxide particles is also affecting the reduction of surface area. The results of pore size distribution also support the findings of the surface area measurement, wherein the pore volume of $AlPO_4$ decreased with the addition of cobalt precursors. All the catalysts show unimodal pore size distribution. It is interesting to note that the surface area, pore volume and pore size of the CoA catalyst are much lower than that of the CoN and CoCl. The pore size distribution patterns shown in Fig. 1, reveal that the homogeneously distributed larger cobalt particles on CoN and CoCl catalysts could block small pores of $AlPO_4$ or deposition in inner pore resulted in the decrease of surface area and eventually increased average pore diameter. However, well-dispersed cobalt particles on CoA catalyst decreased the surface area by deposited cobalt oxides in the inside pore of $AlPO_4$ preferentially resulting in the decrease of average pore diameter. In general, since the large pore diameter of support is beneficial for FTS activity and selectivity to heavy hydrocarbon formation due to the facile reducibility of cobalt species [19–22,32], laboratory-made $AlPO_4$ showing high pore diameter of around 20 nm is a good candidate for the development of Fischer–Tropsch catalyst.

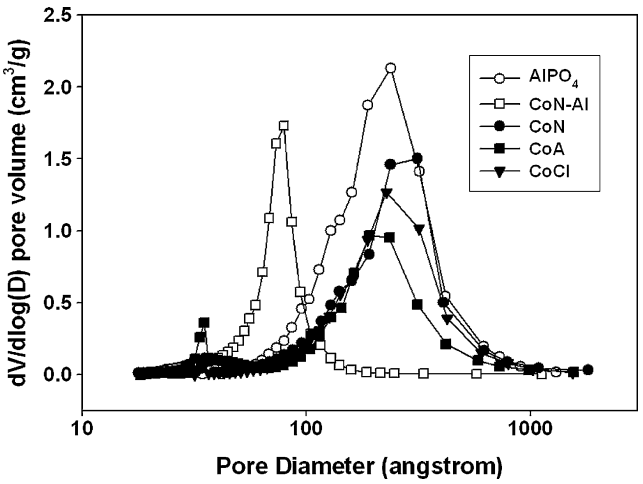

Fig. 1. Pore size distribution of $Co/AlPO_4$ catalysts prepared with three different cobalt precursors, Co/Al_2O_3 and $AlPO_4$ support.

Table 1
Physical properties of $Co/AlPO_4$ and Co/Al_2O_3 catalysts.

Notation[a]	Surface area (m^2/g)	Pore volume (cm^3/g)	Pore size (nm)
$AlPO_4$	173	1.02	19.4
CoN–Al[b]	139	0.33	6.7
CoN	122	0.71	20.1
CoA	101	0.47	14.9
CoCl	116	0.61	20.6

[a] The notation of $Co/AlPO_4$ catalysts like CoN, CoA and CoCl catalysts denotes the catalysts prepared from three different cobalt precursors such as nitrate, acetate and chloride, respectively.

[b] CoN–Al stands for the Co/Al_2O_3 (Catapal B with a surface area of 200 m^2/g) catalyst prepared from cobalt nitrate precursor.

3.2. Crystalline phases of cobalt species and their morphology

The XRD patterns of the CoN–Al and $Co/AlPO_4$ catalysts are shown in Fig. 2(a). The diffraction patterns suggest that $AlPO_4$ support is found to be in the amorphous phase. All the catalysts show the characteristic reflection peak at $2\theta = 36.8°$ due to the presence of Co_3O_4 phase except for CoA catalyst. The particle size of Co_3O_4 calculated by using the X-ray line broadening method with the help of Scherrer's equation is given in Table 2. The average crystallite size of Co_3O_4 for the CoCl catalyst is found to be more than two times larger than that of the CoN catalyst. But, no X-ray detectable cobalt oxide peaks are observed on CoA catalyst. Girardon et al. [33] also reported the amorphous nature of silica supported cobalt catalysts prepared using the cobalt acetate precursor and they have shown that the high exothermicity of cobalt acetate decomposition leads primarily to amorphous and difficultly reducible cobalt silicate. The present XRD analysis suggests that there is no new compound formed between the cobalt oxide and aluminum phosphate. Therefore, the result on CoA reveals the presence of the well-dispersed cobalt particles in amorphous phase. The average crystallite size of cobalt oxide on CoN–Al catalyst was 20.5 nm which is larger than that of CoN catalyst. To identify the phases of cobalt species

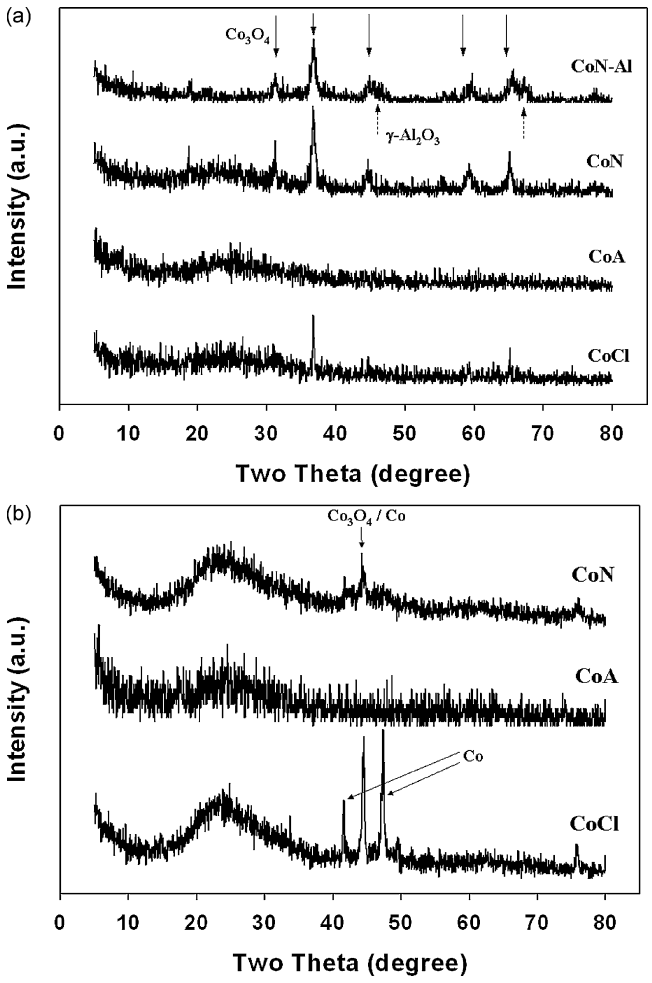

Fig. 2. XRD patterns of $Co/AlPO_4$ catalysts prepared with three different cobalt precursors and Co/Al_2O_3 catalyst. (a) Calcined catalysts, (b) reduced and subsequently passivated catalysts.

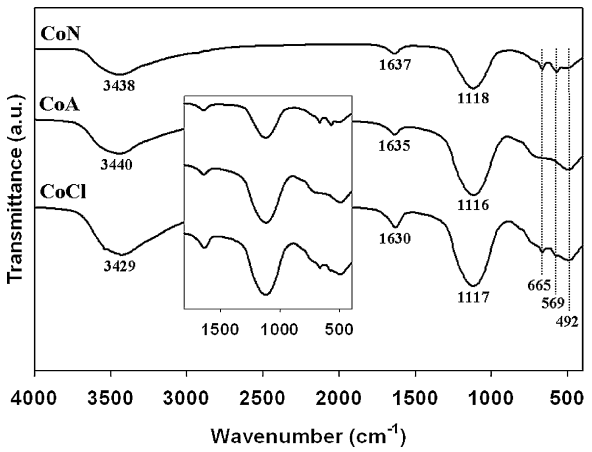

Fig. 3. FT-IR spectra of calcined $Co/AlPO_4$ catalysts prepared with three different cobalt precursors.

of $Co/AlPO_4$ catalysts in the reduced state, the XRD analyses of the catalysts after reduction with hydrogen and successive passivation with 0.1%O_2/He have been carried out and the results are shown in Fig. 2(b). Interestingly, the CoCl catalyst shows intense XRD peaks for Co_3O_4 and Co metal phases. The reflections due to metallic cobalt are more dominant in the CoCl catalyst which is correlated with a large cobalt particle size and very weak interaction with $AlPO_4$ support by possessing the character of unsupported cobalt chloride species [14,15].

The morphological nature of cobalt on $Co/AlPO_4$ was also investigated by using the SEM and EDS analysis. The granular type particles were observed in all $Co/AlPO_4$ catalysts, especially for the CoA catalyst with much smaller particle size (not shown here). The EDS analysis with a sampling depth of 1–2 μm reveals that the cobalt oxides were distributed mainly on the catalyst surface especially for CoN catalysts (the weight ratio of Co/(Al+P) is 28.9, 10.7 and 26.4% for CoN, CoA and CoCl, respectively). On the CoA catalyst, in contrary, cobalt oxides were dispersed in the inner deep pore of $AlPO_4$ homogeneously with a strong metal–support interaction (low mobility during the calcination step) which is also supported by the abrupt decrease of surface area and its high value in pore volume as shown in Fig. 1 and Table 1. Interestingly, the residue of Cl (3.8 wt.%) on CoCl catalyst was not removed efficiently even after calcination treatment and its existence might have affected the aggregation of cobalt particles by a sintering phenomena with the altered mobility of cobalt species due to the water generated during reduction step [34,35]. The TEM images of calcined $Co/AlPO_4$ catalysts prepared by using different cobalt precursors suggest that cobalt oxides are dispersed uniformly on the $AlPO_4$ (not shown here). The sphere type particles on CoN catalyst were found to be above 10 nm in size. The particle sizes for CoCl catalyst are found to be a little bit larger than that of CoN catalyst. The TEM images of CoN and CoA catalysts reveal that cobalt oxide is well dispersed on $AlPO_4$ where as CoCl catalyst shows non-uniform distribution of cobalt oxide.

The FT-IR analysis for the calcined $Co/AlPO_4$ catalysts was carried out to confirm the state of hydroxyl groups on $AlPO_4$ and the Co–O formation and the results are shown in Fig. 3. A broad band centered at ~3500 cm^{-1} is attributed to the isolated OH stretching vibration and the vibration band at ~1640 cm^{-1} is due to the H_2O molecule (HOH). The band at around 1118 and 492 cm^{-1} could be attributed to the triply degenerate P–O stretching vibration mode and to the triply degenerate O–P–O bending vibration mode of tetrahedral $(PO_4)^{3-}$, respectively [26,34,36]. Interestingly, the observed well-dispersed cobalt oxides on CoN catalyst also showed intense vibration band at 665 and 569 cm^{-1} which is assigned to the Co–O absorption band [36,37]. The cobalt oxide with crystalline phase on CoN catalyst is responsible for showing high reduction degree and high activity on FTS reaction.

Table 2
Summary of cobalt particle size characterized by XRD and H_2 chemisorption.

Notation	XRD	O_2 titration	H_2 chemisorption			XPS (binding energy/eV)	
	Particle size of Co_3O_4 (nm)	Reduction degree (%)	Surface area (m^2/g Co-metal)	Uncorrected particle size (nm)	Corrected particle size (nm)[a]	Co $2p_{3/2}$	P 2p
CoN–Al	20.5	55.8	30.5	27.4	15.3	779.1	–
CoN	15.6	65.9	43.0	15.7	10.3	779.1	133.9
CoA	Amorphous phases – not detectable by XRD and H_2 chemisorption					781.2	133.6
CoCl	35.3	41.5	1.7	398.0	165.3	781.2	133.8

[a] The particle size was correlated by reconsidering the reduction degree of cobalt oxides by O_2 titration method.

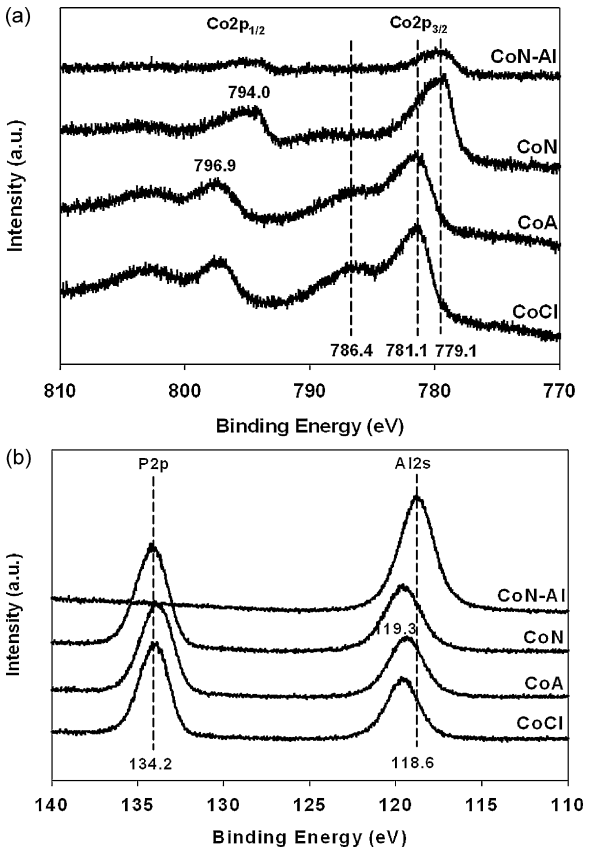

Fig. 4. XPS analysis of $Co/AlPO_4$ catalysts prepared with three different cobalt precursors and Co/Al_2O_3 catalyst. (a) Binding energy vs. intensity of Co $2p_{3/2}$ and Co $2p_{1/2}$; (b) binding energy vs. intensity of P 2p and Al 2s.

The surface cobalt species after calcination were further characterized by XPS analysis and the results are shown in Fig. 4 and Table 2. The characteristic Co $2p_{3/2}$, P 2p and Al 2s peaks were observed in all catalysts at the binding energy (BE) of around 780, 134 and 119 eV, respectively. The high intensity of Co $2p_{3/2}$ peak was observed on $Co/AlPO_4$ catalyst compared to CoN–Al catalyst. It suggests that smaller cobalt particles could be formed on $AlPO_4$ support compared to Al_2O_3 support or the high concentration of cobalt particles on the outer surface of $AlPO_4$ due to the possible migration of cobalt oxides during the calcination step. The intensity ratio of Co/Al from XPS is also suggesting the formation of small cobalt particles in $AlPO_4$ support. This is further confirmed by SEM-EDS analysis like when a high weight ratio (28.9%) of Co/(Al+P) is observed for CoN catalyst. The experimental electron intensity ratio for Co and Al (I_{Co}/I_{Al}) was correlated with cobalt particle size similar to that has been established by many researchers [2,21,22,38]. With the increase of I_{Co}/I_{Al} ratio, the particle size of cobalt decreases with the assumption of monolayer coverage of cobalt species. Although the calculated particle size from XPS peak intensity ratio is not well matched due to agglomeration of particles and heterogeneous distribution, the I_{Co}/I_{Al} values could offer some clues to estimate the cobalt particle size and its distribution. The ratio of I_{Co}/I_{Al} calculated from the spectra shown in Fig. 4 (Co $2p_{3/2}$ and Al 2s) on our samples is 0.34, 1.92, 1.84 1.81 for CoN–Al, CoN, CoA and CoCl catalysts, respectively. Compared with the outer surface concentration from SEM and EDS analysis, the particle size is much smaller on $Co/AlPO_4$ especially for CoA catalyst than the one obtained for CoN–Al catalyst even though the former show high concentration of cobalt on the outer surface of $AlPO_4$. The character of uneven particle size distribution of cobalt species on CoN–Al catalyst with a presence of 5 nm in particle size is also observed [39]. Furthermore, the shift on BE and the satellite peak intensity of Co $2p_{3/2}$ can be useful information in understanding the catalyst; e.g. BE of Co $2p_{3/2}$ around 780 eV is related to the fully oxidized Co_3O_4 particles and satellite peak at somewhat higher BE around 786 eV can be attributed to the localized amorphous-phase Co^{2+} [2,21,22,38]. The presence of satellite peak is generally related to the difficult reducibility of cobalt species and eventually showing a low FTS activity. As shown in Fig. 4, the CoN–Al and CoN catalysts only show a main peak at 779.1 eV assigned to Co_3O_4 particles, however, the satellite peak observed in the case of CoA and CoCl catalysts is of high intensity. The shift to a lower BE on CoN catalyst is beneficial for getting a high FTS activity compared to that of CoA and CoCl catalysts.

3.3. Reducibility of cobalt species and their particle size on $Co/AlPO_4$ catalysts

The H_2 chemisorption on cobalt-based catalysts provides valuable and quantitative information such as the number of cobalt metal sites, cobalt dispersion and its average particle size. It was found that CO chemisorption on cobalt catalysts was non-activated and less reversible than hydrogen chemisorption [40,41]. To verify the cobalt particle size, therefore, H_2 chemisorption was carried over $Co/AlPO_4$ catalysts. The results of H_2 chemisorption including metallic surface area and particle size corrected by using the reduction degree measured by O_2 titration are presented in Table 2. The cobalt species particle size (Co_3O_4 at $2\theta = 36.8^\circ$) calculated from XRD with the value of full width at half maximum (FWHM) was found to be 15.6 and 35.3 nm for CoN and CoCl catalysts, respectively which match well with the cobalt particle size measured from H_2 chemisorption for $Co/AlPO_4$ catalyst. A cobalt particle size (10.3 nm) of CoN is found to be lower than the corresponding CoCl (165.3 nm) and the surface area of cobalt metal of 43.0 m^2/g Co-metal is also found to be higher for CoN catalyst than other catalysts discussed. The large particle size observed on CoCl by H_2 chemisorption is probably due to the Cl residue (confirmed by SEM and EDS analysis) which could induce aggregation of cobalt particles during reduction step or inhibition of dissociative adsorption of H_2 due to the electron donating property of Cl residue [32,35]. These results are also confirmed by XRD (Fig. 2(b)) analysis. For comparison, the cobalt particle size of CoN–Al is also included in Table 2 and it is somewhat larger than that of CoN catalyst. The degree of reduction of cobalt species is higher on CoN (65.9%) compared to that of CoCl (41.5%) and CoN–Al (55.8%). This observation was further substantiated by the results of XPS analysis. The catalysts showing a high peak intensity of Co $2p_{3/2}$ satellite peak at around 786 eV show a low reducibility which is attributed to the localized amorphous-phase Co^{2+}. Therefore, a facile reducibility was observed on CoCl catalyst by TPR experiment, however, the reduction degree of that was measured by O_2 titration is somewhat lower due to the presence of a localized amorphous phase. Although the turn-over frequency (TOF) is known to be constant above the particle size of 6–8 nm [42], the differences in cobalt particle size and reducibility could affect the catalytic activity and product distribution by changing the adsorption properties of CO and H_2. The metallic surface area measured from H_2 chemisorption provides valuable information such as the surface concentration and competitive adsorption properties of CO and H_2. CO-rich and H_2-deficient environment seems to be responsible for the low CO conversion and high selectivity to C_8+. In addition, the degree of reduction of cobalt oxides also alters the electronic state of reduced cobalt metal, i.e. highly reduced cobalt particles with appropriate particle size above 10 nm could affect the easy activation of CO molecule and H_2 [7,12,42] which resulted in showing the high catalytic activity on CoN catalyst.

TPR studies were carried out to investigate the reducibility of the $Co/AlPO_4$ catalysts and the results are shown in Fig. 5. The TPR profile of CoN catalyst exhibits two clearly distinct peaks at 390 °C

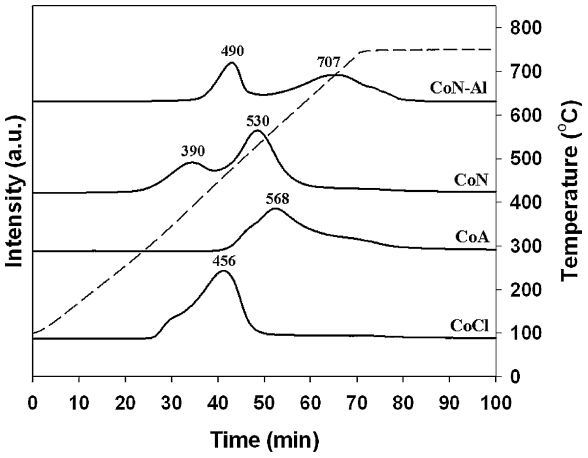

Fig. 5. TPR profiles of $Co/AlPO_4$ catalysts prepared with three different cobalt precursors and Co/Al_2O_3 catalyst.

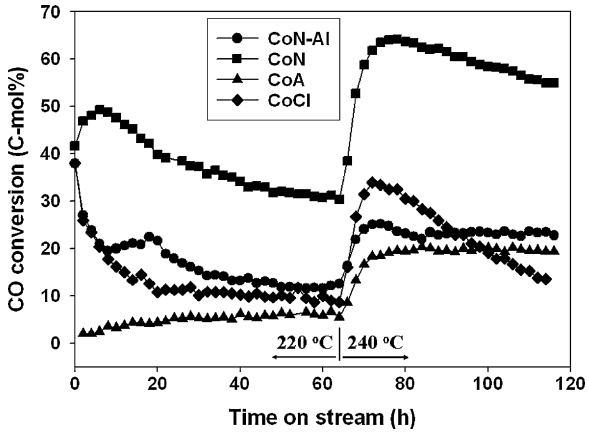

Fig. 7. Variation of CO conversion with time on stream (h) on $Co/AlPO_4$ catalysts prepared with three different cobalt precursors and Co/Al_2O_3 catalyst. Reaction conditions: T = 220–240 °C; P = 2.0 MPa; SV (l/kg_{cat}/h) = 2000; feed compositions of $H_2/CO/CO_2/Ar$ (mol%) = 57.3/28.4/9.3/5.0.

and 530 °C. The first peak is attributed to the reduction of Co_3O_4 to CoO and the second peak is assigned to the reduction of CoO to metallic cobalt. The TPR profile of CoCl catalyst also shows two reduction peaks but at much lower temperature with a shoulder around 350 °C and an intense second peak at 456 °C compared to that of CoN catalyst. The TPR profile of CoA catalyst did not show any reduction peak below 400 °C, and a broad peak appeared at 568 °C with a shoulder at low temperature. The low peak intensity on CoA suggests the difficult reduction and non-reducible cobalt particles could be formed due to the formation of difficulty reducible cobalt species during calcination step which is confirmed by FT-IR, XPS and XRD analysis. Furthermore, the CoN–Al catalyst shows the two distinct reduction peaks at much higher temperature at 490 and 707 °C. The peak at 707 °C corresponds to the cobalt–aluminate formation which is not observed in the case of $AlPO_4$ supported catalysts. This means that the modification of Al_2O_3 with PO_4 species decreases the salt–support interaction. The reduced salt–support interaction on $AlPO_4$ support and homogeneous particle size distribution of cobalt oxides compared to the uneven distribution on CoN–Al catalyst [31,39] is responsible for the formation of smaller average particles on CoN catalyst.

The electronic states of reduced cobalt species and their structural characters are investigated by DRIFT experiment by observing the types of adsorbed CO molecules and the results are shown in Fig. 6. In general, the adsorbed CO molecules show distinctive absorption band at around 1930–1980, 2030–2050, 2050–2070 and above 2110 cm^{-1} for a bridged-type CO adsorption on metallic cobalt, a linear-type CO adsorption on metallic cobalt, CO adsorption on metallic cobalt (Co^0) with less electron-donor properties ($Co^{\delta+}$ sites) and residual gaseous CO molecules respectively [2,7,12,43]. In general, the bridged-type and linear-type CO molecules are active species on FTS reaction due to the low activation energy for CO hydrogenation. The high electron density on the reduced cobalt species could increase the availability of d-orbital electron by electron back donation from metal particle to the adsorbed CO molecule and eventually reduce the C–O bonding energy which is shifting to lower CO frequency [2,7]. On our samples, the intense peaks for the bridged-type and the linear-type CO molecules on the hexagonal cobalt phase were observed on the CoN and CoCl catalysts. The CoA catalyst shows no peak in this absorption range due to the difficulty in reduction. Although CoCl catalyst shows no intense peaks for bridged-type and the linear-type CO molecules, the peak at around 2059.6 cm^{-1} assigned to the electron-deficient $Co^{\delta+}$ sites with cubic cobalt phase is larger [43]. These observations are well matched with the results of XPS, TPR and degree of reduction. Interestingly, the bridged-type CO adsorption band at 1936.2 cm^{-1} and the linear-type CO adsorption band at 2034.6 cm^{-1} is intense and shifted to low energy on the CoN catalyst showing high reducibility due to the presence of electron-rich cobalt species. The highly reducible cobalt species on CoN catalyst shows low reduction temperature (confirmed by TPR in Fig. 5), intense bridged-type and the linear-type CO adsorption band (confirmed by DRIFT in Fig. 6) and small satellite peak intensity of Co $2p_{3/2}$.

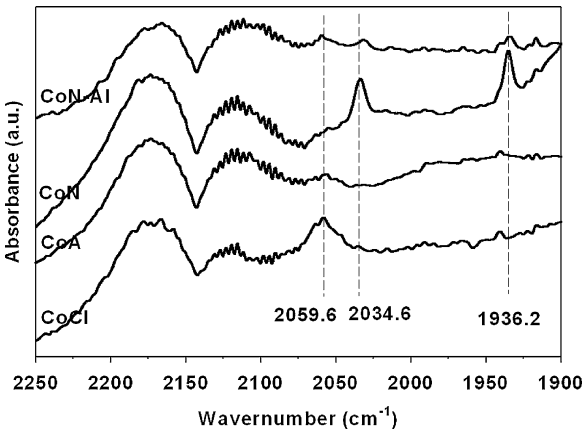

Fig. 6. DRIFT spectra of adsorbed CO on the reduced $Co/AlPO_4$ catalysts prepared with three different cobalt precursors and Co/Al_2O_3 catalyst.

The results of TPR analysis, particle size analysis from XRD, electronic and surface structural properties of cobalt species by XPS analyses and adsorbed CO FT-IR, and H_2 chemisorption confirm that the CoN catalyst is responsible for showing good catalytic activities due to the facile reducibility at low temperature with appropriate cobalt particle size and high electron density as discussed in the following section.

3.4. Catalytic activity on $Co/AlPO_4$ catalysts and filamentous carbon formation

The variation of catalytic activity during FTS on $Co/AlPO_4$ catalysts with time on stream is reported in Fig. 7 and the product distribution is presented in Table 3. At the reaction temperature of 220 °C, the initial activity of CoN catalyst is much higher than the other catalysts and it shows a higher CO conversion at reaction temperature of 240 °C. The cobalt nitrate precursor on CoN catalyst is much easily reduced at low temperature with the formation

Table 3
Conversion and product distribution on $Co/AlPO_4$ with three different cobalt precursors and Co/Al_2O_3 catalysts.

Notation	Cobalt precursor	Temp. (°C)	Conversion of CO	Initial TOF (converted CO molecules/surface Co atom/s) $\times 10^{-2}$	Selectivity (C-mol%)				
					C_1	C_2–C_4	C_5–C_7	C_8^+	O/(O+P)[a]
CoN–Al	Nitrate	220	11.8	1.24	15.0	11.9	12.3	60.8	35.3
		240	23.3	1.15	18.2	16.7	16.8	48.3	32.8
CoN	Nitrate	220	31.4	1.61	16.7	14.1	14.9	54.3	40.8
		240	57.4	2.07	20.6	16.5	17.9	45.0	29.1
CoA	Acetate	220	6.1	–	16.7	16.9	14.1	52.3	37.8
		240	19.8	–	22.7	19.9	17.1	40.3	22.0
CoCl	Chloride	220	9.9	2.14	29.1	24.1	10.4	36.4	18.8
		240	17.0	2.80	39.9	23.4	9.9	26.8	11.6

[a] The content of olefin [O/(O+P); olefin/(olefin + paraffin) × 100] was calculated in the range of C_2–C_4 hydrocarbons.

of electron-sufficient state and highly dispersed on $AlPO_4$ showing high FTS activity. The CoA and CoCl catalysts have shown much lower conversion than that of CoN catalyst. Among all the catalysts, CoA catalyst shows the lowest CO conversion during FTS. The CO_2 formation in all our catalysts is lower than 1.0 mol% due to the low water-gas shift (WGS) activity on cobalt-based catalysts. The initial TOF values are calculated by using the surface area of metallic cobalt characterized by H_2 chemisorption. The low initial TOF (defined as converted CO molecules/surface Co atom/s) of around 0.0124 at 220 °C was observed on CoN–Al catalyst due to the presence of small cobalt particles below 5 nm. The initial TOF value of 0.0214 is higher on CoCl catalyst respectively than the results reported by Bezemer et al. [42] due to the presence of cobalt species possessing less electron-donor properties ($Co^{\delta+}$ sites) which is eventually responsible for the high selectivity to CH_4 [2,7,12,21,22,38,39,43]. The high initial TOF value of 0.0161 was observed on CoN catalyst showing a homogeneous cobalt distribution on the large pore $AlPO_4$ support and a high reducibility with electron-rich cobalt surfaces. These trends with activity variation on different FTS catalysts are also similar at high temperature of 240 °C. The observed initial TOF on $Co/AlPO_4$ catalysts could be affected by cobalt particle size as well as pore size of catalysts and deactivation by filamentous carbon formed [44,45]. The activity changes with time on stream (deactivation rate) could be correlated with the sintering phenomena of cobalt particles (reconstruction and aggregation) and possible oxidation by water formed as well as filamentous carbon formation during FTS reaction and eventually alters the TOF values with time on stream.

Fig. 8 shows TEM images of $Co/AlPO_4$ catalysts after reaction for 120 h on stream and their surface composition was also analyzed by EDS for CoN catalyst. Interestingly, all samples show growth of filamentous carbon initiated from large cobalt particles. The EDS analysis reveals that the filamentous materials are composed of carbon and the cobalt particle was encapsulated at the end of filamentous carbon. Even though the growth of filamentous carbon was found to be severe on CoN and CoA catalysts, the reactive cobalt particles above 10 nm still exist abundantly on those catalysts which are responsible for a high CO conversion after long-term experiments. Furthermore, the cobalt particle size on CoA catalyst is much smaller than that of others in the reduced states (confirmed by XPS and TEM) and a homogeneous distribution of the amorphous phase is responsible for the facile aggregation of cobalt particles during FTS reaction and eventually formation of filamentous carbon was enhanced. The structural and textural properties of catalytic filamentous carbon depend on many factors like the catalyst composition, gaseous precursor and the temperature. Normally reaction temperatures greater than 500 °C are required for the carbon filament formation [46]. Literature is abundant with the information on the preparation of filamentous carbon. For example, high loaded $Ni–Al_2O_3$, $Ni–Cu–Al_2O_3$, $Co–Al_2O_3$ and Fe-containing co-precipitated catalysts have been used for the preparation of filamentous carbon [46] by Bouduard reaction or CO disproportionation reaction. These catalysts have longer life and allow carbons to be produced in larger quantities. But the temperatures required are of the order of 500–675 °C. In this context, the preparation of carbon filaments at lower temperature such as 240 °C assumes considerable significance. The filamentous carbon in $Co/AlPO_4$ catalyst was composed of less ordered multi-walls which were initiated from the large cobalt particles at the end of filamentous carbon. According to Wang and Ruckenstein [47], filamentous carbon formation is favorable in the presence of a strong interaction between the cobalt atom and the support, when an ordered structure templates into an ordered carbon nucleus. When the interaction is low, the large particles of cobalt formed are less ordered and numerous carbon nuclei will be formed. The carbon deposits will coalesce during their growth, thus restricting the formation of fibers.

To verify the character of filamentous carbons, Raman spectroscopy is carried over the used $Co/AlPO_4$ catalysts as shown in Fig. 9. In the case of hexagonal graphite [46,47], the main band at around 1585 cm^{-1} is attributed to the in-plane displacement of carbon atoms (G-mode) and new band at around 1300 cm^{-1} appears with the increase of disorder in graphite structure (D-mode). Therefore, in our samples, the observed band at around 1286 and 1591 cm^{-1} reveals a disordered filamentous carbon formation due to the low reaction temperature below 240 °C. The aggregation of cobalt particles was also observed on all the samples, however, the particle size was much larger on CoCl catalyst after FTS reaction. The aggregation of cobalt particles as well as growth of filamentous carbon could be an important reason for the deactivation of $Co/AlPO_4$ catalysts.

The CoN and CoCl catalysts show an abrupt decrease in activity which can be attributed to the carbon deposition including filamentous carbons, however, even after forming filamentous carbon on CoN and CoA catalysts, a large portion of active cobalt around 10 nm in size exists which is responsible for the catalytic activity of these catalysts. Therefore, CoN catalyst showing high reducibility and proper cobalt particle size is responsible for the low deactivation rate and high CO conversion by enhancing the easy dissociation of H_2 and facile formation of active CO species such as a bridged type on the reduced cobalt metal particles with electron-rich state. Although the presence of large cobalt particles and their facile reducibility at low temperature is observed on CoCl catalyst, the fast deactivation rate and low CO conversion was observed due to the possible poisoning by chlorine residue which is not easily removed by calcination and reduction steps and also carbon deposition. Interestingly, CoA catalyst showing difficult reduction property and smallest cobalt particle size shows a low CO conversion and stable catalytic activity in spite of filamentous carbon formation during the FTS reaction and it could be attributed to the suppression of sintering and reoxidation phenomena during

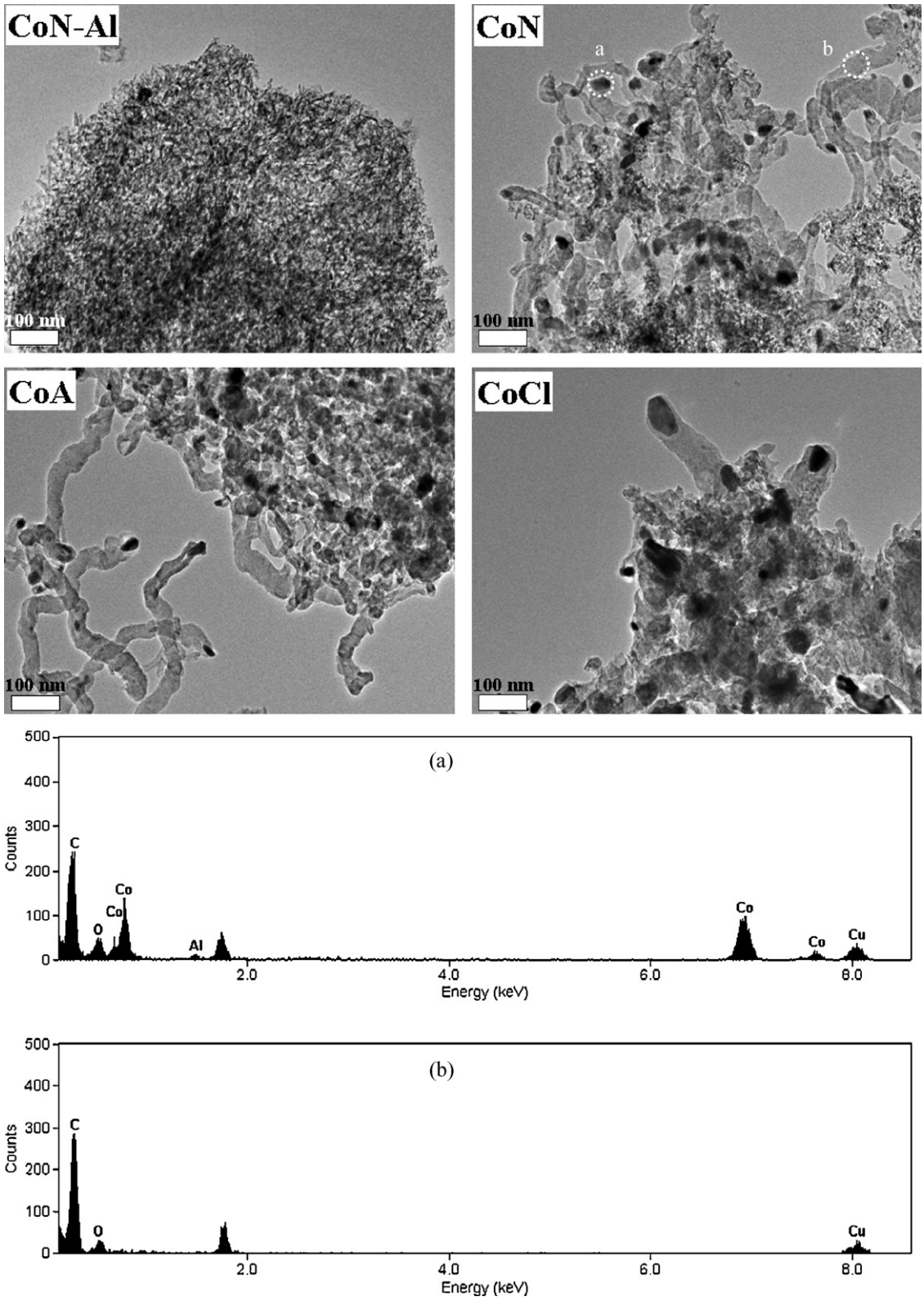

Fig. 8. TEM images of used $Co/AlPO_4$ catalysts prepared with three different cobalt precursors and Co/Al_2O_3 catalyst, and EDS analysis for cobalt particle (point a) and filamentous carbon (point b) on CoN catalyst.

FTS reaction [15]. In order to compare the catalytic activity with $Co/AlPO_4$ catalysts, the corresponding data on cobalt supported on Al_2O_3 is also given in Table 3 and Fig. 7. The results suggest that CoN–Al shows a much lower CO conversion with high selectivity to C_8+ at the reaction temperatures of 220 °C and 240 °C than that of $Co/AlPO_4$ catalysts due to the uneven distribution of cobalt particles and diffusion-limitation in small pore [3,48]. The enhanced activity on $Co/AlPO_4$ catalysts can be ascribed to the decreased cobalt–aluminate formation, thereby more cobalt is available for the FTS reaction. Although CoN catalyst exhibits higher C_1 selectiv-

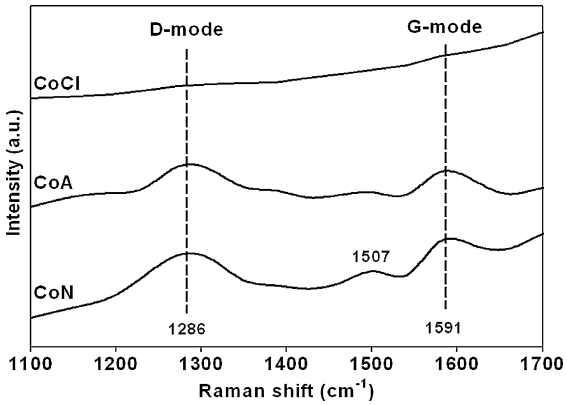

Fig. 9. Raman spectroscopy on the used $Co/AlPO_4$ catalysts prepared from three different cobalt precursors.

ity than that of CoN–Al catalyst, the CO conversion is three times higher on CoN catalyst at 220 °C. The high value for the olefin content in C_2–C_4 hydrocarbons on CoN catalyst correlated well with C_8+ selectivity due to the possible diffusion-enhanced readsorption of α-olefins [3] in large pore of CoN catalyst. In our previous work [45], it was shown that the addition of Ru to CoN catalyst further enhances the CO conversion and C_8+ selectivity without filamentous carbon formation due to the facile hydrogen spill-over activity. The low CO conversion and lack of formation of filamentous carbon on CoN–Al catalyst are attributed to difficulty in reduction of cobalt oxides due to strong interaction of cobalt species with Al_2O_3 support. Furthermore, the cobalt precursors could alter the solution pH during the preparation step and results in changing the particle size distribution and reducibility and finally change the CO conversion and product distribution [39,48]. Furthermore, in our recent publication [49], the phosphorous-modified Al_2O_3 support for cobalt-based FTS catalyst is reported to obtain high catalytic activity and selectivity to C_5+ due to the homogeneous distribution of cobalt particles and their redispersion phenomena during FTS reaction by the partial transformation of Al_2O_3 surface to aluminum phosphate.

The selectivity of C_8+ was found to be higher for the CoN catalyst and the order of C_8+ selectivity is as follows; CoN > CoA > CoCl. It is interesting to note that the CoCl catalyst exhibits higher C_1 and C_2–C_4 selectivities than the other $Co/AlPO_4$ catalysts in spite of facile reducibility and larger particle size. The lower C_8+ selectivity on CoCl catalyst could be attributed to the chlorine residue which may enhance sintering of the cobalt particles and the presence of partially reduced cobalt species such as the electron-deficient $Co^{\delta+}$ sites with cubic cobalt phase which is responsible for the high CH_4 selectivity [21,22,38,43], and abrupt deactivation by forming a carbon deposition that is responsible for the difficult activation of CO, and enhancement of C_1 selectivity. The CoN catalyst shows higher value for O/(O+P) compared to the other catalysts. The C_8+ selectivity correlated with the reducibility of cobalt particles with proper electronic state (confirmed by the results of XPS and DRIFT) which enhanced with the increase of reduction degree as shown in Table 2 except for the CoCl catalyst. Furthermore, the ease diffusion of reactants and products in the large pore of $AlPO_4$ is also responsible for the high C_8+ selectivity by facile secondary reaction of α-olefins [3,48]. The high activity on CoN catalyst is attributed to the enhancement of reduction degree with high surface area of metallic cobalt with proper electronic states which is enhancing the dissociative adsorption of CO (linear and bridged-type CO adsorption) and large pore diameter of $AlPO_4$ support which is beneficial for the facile secondary reaction.

4. Conclusions

The use of $AlPO_4$ as a support for cobalt-based catalysts exhibits better catalytic performance during FTS than the corresponding Co/Al_2O_3 catalyst. The information obtained by the characterization such as XRD, TPR, FT-IR and DRIFT, XPS, TEM, Raman and chemisorption analysis further support the enhanced catalytic properties. The $Co/AlPO_4$ catalysts prepared from cobalt nitrate precursor show higher CO conversion and C_8+ selectivity than the catalysts prepared from the corresponding precursors such as acetate and chloride due to the facile reduction properties with a proper electronic state of reduced cobalt species and large pore diameter with the diffusion-enhanced re-adsorption of α-olefins. The higher selectivity of C_8+ is found to be in the order of CoN > CoA > CoCl catalyst. Interestingly, all $Co/AlPO_4$ catalysts showed a filamentous carbon formation which is responsible for the abrupt decrease of catalytic activity compared to that of Co/Al_2O_3 catalyst. The differences in the catalytic properties exhibited by $Co/AlPO_4$ catalysts are attributed to the cobalt particle size, reducibility with different electronic states of cobalt species which is enhancing the dissociative adsorption of CO molecule (linear- and bridged-type CO species) and a large pore size of $AlPO_4$ with a facile diffusion of formed hydrocarbons as well as filamentous carbon formation.

Acknowledgements

The authors would like to acknowledge the financial support of KEMCO and GTL Technology Development Consortium (Korea National Oil Corp., Daelim Industrial Co., Ltd, Doosan Mecatec Co., Ltd, Hyundai Engineering Co. Ltd and SK Energy Co. Ltd) under "Energy & Resources Technology Development Programs" of the Ministry of Knowledge Economy, Republic of Korea. Dr. K.V.R. Chary thanks the Korea Federation of Science and Technology (KOFTS) for the visiting scientist fellowship under the Brain Pool Fellowship program.

References

[1] R.J. Madon, E. Iglesisa, J. Catal. 139 (1993) 576.
[2] A.Y. Khodakov, W. Chu, P. Fongarland, Chem. Rev. 107 (2007) 1692.
[3] E. Iglesia, Appl. Catal. A 161 (1997) 59.
[4] M.E. Dry, Catal. Today 71 (2002) 227.
[5] R. Oukaci, A.H. Singleton, J.G. Goodwin Jr., Appl. Catal. A 186 (1999) 129.
[6] B.H. Davis, Top. Catal. 32 (2005) 143.
[7] J.W. Bae, I.G. Kim, J.S. Lee, K.H. Lee, E.J. Jang, Appl. Catal. A 240 (2003) 129.
[8] H. Xiong, Y. Zhang, W. Wang, J. Li, Catal. Commun. 6 (2005) 512.
[9] Z. Yu, Øyvind Borg, E. De Chen, A. Rytter, Holmen, Topics Catal. 45 (2007) 69.
[10] O. Borg, S. Eri, E.A. Blekkan, S. Storsaeter, H. Wigum, E. Rytter, A. Holmen, J. Catal. 248 (2007) 89.
[11] G. Jacobs, T.K. Das, Y. Zhang, J. Li, G. Racoillet, B.H. Davis, Appl. Catal. A 233 (2002) 263.
[12] J. Zhang, J. Chen, J. Ren, Y. Sun, Appl. Catal. A 243 (2003) 121.
[13] A. Martinez, J. Rollan, M.A. Arribas, H.S. Cerqueira, A.F. Costa, E.F.S. Aguiar, J. Catal. 249 (2007) 162.
[14] E. van Steen, G.S. Sewell, R.A. Makhothe, C. Micklethwaite, H. Manstein, M. de Lange, C.T. O'Connor, J. Catal. 162 (1996) 220.
[15] M.P. Rosynek, C.A. Polansky, Appl. Catal. 73 (1991) 97.
[16] B. Ernst, S. Libs, P. Chaumette, P. Kinnemann, Appl. Catal. A 186 (1999) 145.
[17] N. Tsubaki, S. Sun, K. Fujimoto, J. Catal. 199 (2001) 236.
[18] A.M. Hilmen, D. Schanke, A. Holmen, Catal. Lett. 38 (1996) 143.
[19] A.M. Saib, M. Claeys, E. van Steen, Catal. Today 71 (2002) 395.
[20] A.Y. Khodakov, A. Griboval-Constant, R. Bechara, F. Villain, J. Phys. Chem. B 105 (2001) 9805.
[21] A.Y. Khodakov, A. Griboval-Constant, R. Bechara, V.L. Zholobenko, J. Catal. 206 (2002) 230.
[22] A.Y. Khodakov, J. Lynch, D. Bazin, B. Rebours, N. Zanier, B. Moisson, P. Chaumette, J. Catal. 168 (1997) 16.
[23] G. Marcelin, R.G. Vogel, H.E. Swift, J. Catal. 83 (1983) 42.
[24] P.S. Kuo, B.L. Yang, J. Catal. 117 (1989) 301.
[25] L. Pellettier, D.D.S. Liu, Appl. Catal. A 317 (2007) 293.
[26] V.S. Kumar, A.H. Padmasri, C.V.V. Satyanarayana, A.K. Reddy, B.D. Raju, K.S. Rama Rao, Catal. Commun. 7 (2006) 745.
[27] F. Yaripour, F. Baghaei, I. Schmidt, J. Perregaard, Catal. Commun. 6 (2005) 542.

[28] K.V.R. Chary, G. Kishan, K. Ramesh, Ch. Praveen Kumar, G. Vidyasagar, Langmuir 19 (2003) 4548.
[29] T.T.P. Cheung, K. Wilcox, M.P. Mc Daneil, M.M. Johnson, C. Bronniman, J. Frye, J. Catal. 102 (1986) 10.
[30] J.M. Campelo, J.M. Marianas, S. Mendioroz, J.A. Pajares, J. Catal. 101 (1986) 484.
[31] R. Iwamoto, J. Grimblot, Adv. Catal. 44 (2000) 417.
[32] C. Lesaint, W.R. Glomm, O. Borg, S. Eri, E. Rytter, G. Oye, Appl. Catal. A 351 (2008) 131.
[33] J.S. Girardon, A. Constant-Griboval, L. Gengembre, P.A. Chernavskii, A.Y. Khodakov, Catal. Today 106 (2005) 161.
[34] T. Gjervan, R. Prestvik, B. Tøtdal, C.E. Lyman, A. Holmen, Catal. Today 65 (2001) 163.
[35] S.H. Song, S.B. Lee, J.W. Bae, P.S. Sai Prasad, K.W. Jun, Y.G. Shul, Catal. Lett. 129 (2009) 233.
[36] F.M. Bautista, J.M. Campelo, A. Garcia, D. Luna, J.M. Marinas, A.A. Romero, G. Colon, J.A. Navio, M. Macias, J. Catal. 179 (1998) 483.
[37] L. Shi, J. Chen, K. Feng, Y. Sun, Fuel 87 (2008) 521.
[38] A.Y. Khodakov, R. Bechara, A. Griboval-Constant, Appl. Catal. A 254 (2003) 273.
[39] J.W. Bae, Y.J. Lee, J.Y. Park, K.W. Jun, Energy Fuels 22 (5) (2008) 2885.
[40] R.C. Reuel, C.H. Bartholomew, J. Catal. 85 (1984) 63.
[41] A.Y. Khodakov, B. Peregryn, A.S. Lermontov, J.S. Girardon, S. Pietrzyk, Catal. Today 106 (2005) 132.
[42] G.L. Bezemer, J.H. Bitter, H.P.C.E. Kuipers, H. Oosterbeek, J.E. Holewijn, X. Xu, F. Kapteijn, A. Jos van Dillen, K.P. de Jong, J. Am. Chem. Soc. 128 (12) (2006) 3956.
[43] D. Song, J. Li, Q. Cai, J. Phys. Chem. C 111 (2007) 18970.
[44] J.H. Oh, J.W. Bae, S.J. Park, P.K. Khanna, K.W. Jun, Catal. Lett. 130 (2009) 403.
[45] J.W. Bae, S.M. Kim, S.J. Park, P.S. Sai Prasad, Y.J. Lee, K.W. Jun, Ind. Eng. Chem. Res. 48 (6) (2009) 3228.
[46] T.V. Reshetenko, L.B. Avdeeva, Z.R. Ismagilov, V.V. Pushkarev, S.V. Cherepanova, A.L. Chuvilin, V.A. Likholobov, Carbon 41 (8) (2003) 1605.
[47] H.Y. Wang, E. Ruckenstein, Carbon 40 (11) (2002) 1911.
[48] S.J. Park, J.W. Bae, J.H. Oh, K.V.R. Chary, P.S. Sai Prasad, K.W. Jun, Y.W. Rhee, J. Mol. Catal. A 298 (2009) 81.
[49] J.W. Bae, S.M. Kim, Y.J. Lee, M.J. Lee, K.W. Jun, Catal. Commun. 10 (2009) 1358.